

Energy Dependence of Intermittency for Charged Hadrons in Au+Au Collisions at RHIC

The STAR Collaboration

Density fluctuations near the QCD critical point can be probed via an intermittency analysis in relativistic heavy-ion collisions. We report the first measurement of intermittency in Au+Au collisions at $\sqrt{s_{\text{NN}}} = 7.7\text{-}200$ GeV measured by the STAR experiment at the Relativistic Heavy Ion Collider (RHIC). The scaled factorial moments of identified charged hadrons are analyzed at mid-rapidity and within the transverse momentum phase space. We observe a power-law behavior of scaled factorial moments in Au+Au collisions and a decrease in the extracted scaling exponent (ν) from peripheral to central collisions. The ν is consistent with a constant for different collision energies in the mid-central (10-40%) collisions. Moreover, the ν in the 0-5% most central Au+Au collisions exhibits a non-monotonic energy dependence that reaches a possible minimum around $\sqrt{s_{\text{NN}}} = 27$ GeV. The physics implications on the QCD phase structure are discussed.

The major goal of the Beam Energy Scan (BES) program at the Relativistic Heavy Ion Collider (RHIC) is to explore the phase diagram of the quantum chromodynamic (QCD) matter. By tuning the collision energies, the QCD phase diagram can be mapped and displayed into a two dimensional plane of temperature (T) versus baryon chemical potential (μ_B) [1–4]. Lattice QCD calculations predict a crossover transition from hadronic matter to a plasma of deconfined quarks and gluons (QGP) at vanishing μ_B [5]. At large μ_B , QCD-based model calculations suggest that the phase transition is of first-order [6]. An important landmark of the QCD phase diagram is the critical end point (CEP), where the first-order phase transition boundary terminates [6–8]. Many efforts have been made to search for the possible CEP in heavy-ion collisions [1, 2, 9–11]. Several measurements from the BES program at RHIC showed a non-monotonic variation with $\sqrt{s_{\text{NN}}}$. These include the net-proton kurtosis [3, 12, 13], the slope of directed flow for protons and net-protons [14], and the Hanbury-Brown–Twiss (HBT) radii [15, 16].

The aim of this work is to look for critical intermittency induced by the CEP [17, 18] in heavy-ion collisions. Upon approaching a critical point, the correlation length of the system diverges and the system becomes scale invariant, or self-similar [19–21]. Based on the 3D-Ising universality class arguments [17, 22, 23], the density-density correlation function for small momentum transfer has a power-law structure, which gives rise to large density fluctuations in heavy-ion collisions [17, 22–24]. Such fluctuations can be probed via an intermittency analysis by utilizing the scaled factorial moments (SFMs) [17, 22, 23, 25, 26]. For this purpose, the D -dimensional phase space is partitioned into M^D equal-sized cells and the observable, q th-order SFM or $F_q(M)$, is defined as follows [17, 18, 27–30]:

$$F_q(M) = \frac{\langle \frac{1}{M^D} \sum_{i=1}^{M^D} n_i(n_i - 1) \cdots (n_i - q + 1) \rangle}{\langle \frac{1}{M^D} \sum_{i=1}^{M^D} n_i \rangle^q}, \quad (1)$$

where M^D is the number of cells in D -dimensional phase

space and n_i is the measured multiplicity of a given event in the i th cell. The angle bracket denotes an average over the events. If a system features self-similar density fluctuations, we expect a power-law behavior of $F_q(M) \propto (M^D)^{\phi_q}$, $M \gg 1$, equivalently, $F_q(M)/M$ scaling, where ϕ_q is called the intermittency index and quantifies the strength of intermittency [17, 22, 23, 25, 27]. A strong $F_2(M)/M$ scaling with $\phi_2 = 0.96 \pm 0.16$ for protons was observed in Si+Si collisions at 158A GeV by the NA49 experiment [25, 27, 31]. In this paper, another type of power-law behavior will be used: $F_q(M) \propto F_2(M)^{\beta_q}$, $M \gg 1$, namely, $F_q(M)/F_2(M)$ scaling, where β_q is the scaling index [18, 32–35]. According to the Ginzburg-Landau (GL) theory [18, 32], the β_q is independent of the details of the critical parameters, thus the $F_q(M)/F_2(M)$ scaling can be measured experimentally and the signal will not be washed out during hadronic evolution. To describe the general consequences of the phase transition, a scaling exponent (ν) is given by $\beta_q \propto (q - 1)^\nu$ [18, 32, 33, 36]. Here, ν also quantifies the strength of intermittency. Near the CEP, the value of ν is predicted to be equal to 1.304 in the entire phase space based on GL theory [18] and equal to 1.0 from the calculations of the 2D Ising model [32, 37].

This letter reports the collision energy and centrality dependence of SFMs and intermittency exponents for identified charged hadrons in Au+Au collisions at RHIC/STAR. The data presented here were obtained from Au+Au collisions at $\sqrt{s_{\text{NN}}} = 7.7, 11.5, 14.5, 19.6, 27, 39, 54.4, 62.4,$ and 200 GeV, recorded by the Solenoidal Tracker at RHIC (STAR) experiment from 2010 to 2017 [38]. These energies correspond to μ_B values ranging from 20 to 420 MeV at chemical freeze-out [38]. The 7.7, 11.5, 39, 62.4, and 200 GeV data were collected in 2010. The 19.6 GeV and 27 GeV data were collected in 2011, and the 14.5 GeV and 54.4 GeV data were collected in 2014 and 2017. All data were obtained using the Time Projection Chamber (TPC) and the Time-of-Flight (TOF) detectors at STAR [39, 40]. Events are selected within a certain Z -position range ($|V_Z| < 30$ cm) from

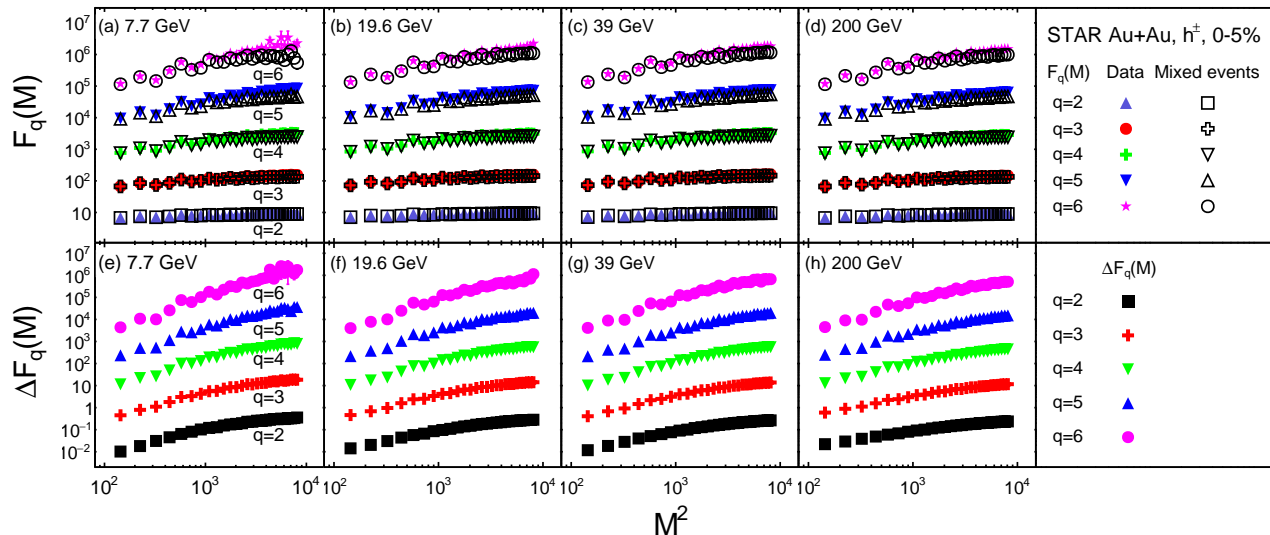


FIG. 1. (a)-(d) The scaled factorial moments, $F_q(M)$ ($q = 2-6$), of identified charged hadron (h^\pm) multiplicity in the most central (0-5%) Au+Au collisions at four example energies in the $\sqrt{s_{NN}} = 7.7-200$ GeV range. Solid (open) markers represent $F_q(M)$ of data (mixed events) as a function of M^2 . (e)-(h) $\Delta F_q(M)$ ($q = 2-6$) as a function of M^2 in the most central (0-5%) Au+Au collisions at four example energies in double-logarithmic scale. Statistical uncertainties are obtained from the Bootstrap method.

the center of the TPC along the beam line ($|V_Z| < 50$ cm for 7.7 GeV) to optimize for the uniformity in the response of the detectors [13]. Background events, which include interactions with the beam pipe, are rejected by requiring a vertex radius V_r less than 2 cm from the center of STAR ($V_r < 1$ cm for 14.5 GeV). To avoid self-correlation [13, 41], the centrality is determined from the uncorrected charged particle multiplicity within a pseudorapidity window of $0.5 < |\eta| < 1$, chosen to be outside the analysis window of $|\eta| < 0.5$. The centrality is represented by the average number of participating nucleons $\langle N_{part} \rangle$ obtained by fitting the reference multiplicity distribution with a Monte Carlo Glauber model [41, 42]. The number of events for $\sqrt{s_{NN}} = 7.7, 11.5, 14.5, 19.6, 27, 39, 54.4, 62.4, \text{ and } 200$ GeV, are 3.3, 6.8, 13.1, 16.2, 32.2, 89.3, 441.7, 46.7, and 236.0 million, respectively.

Charged hadrons, including protons (p), antiprotons (\bar{p}), kaons (K^\pm), and pions (π^\pm), are identified using the TPC and TOF detectors. TPC particle identification is performed using the measured energy loss (dE/dx), with K^\pm and π^\pm requiring a momentum range of $0.2 < p_T < 0.4$ GeV/c, and p and \bar{p} requiring a momentum range of $0.4 < p_T < 0.8$ GeV/c. In addition, the mass squared from the TOF detector is used for particle identification, with K^\pm and π^\pm requiring a momentum range of $0.4 < p_T < 1.6$ GeV/c, and p and \bar{p} requiring a momentum range of $0.8 < p_T < 2.0$ GeV/c. A maximum distance of closest approach (DCA) to the collision vertex of 1 cm is required for each candidate track, which helps to suppress contamination due to weak decays and tracks from secondary vertices [12, 38].

Tracks must have at least 20 points used in track fitting out of the maximum of 45 hits possible in the TPC. To avoid multiple counting of split tracks, more than 52% of the total possible fit points are required. When measuring scaled factorial moments, it is observed that a large number of background effects significantly influence the results [25, 27, 43, 44]. These effects, including the conservation laws, Coulomb repulsion, resonance decays, and experimental acceptance, need to be taken into account in the calculation of the SFMs. In our analysis, the mixed event method is applied to eliminate background contributions [25, 27, 31]. Therefore, an additional observable is defined as $\Delta F_q(M) = F_q(M)^{data} - F_q(M)^{mix}$ [25, 27, 28, 31], where the moments from mixed events representing the background contributions are subtracted from the data. In the following analysis, we will exclusively use $\Delta F_q(M)$ instead of $F_q(M)$.

Experimentally, the values of SFMs are influenced by the efficiency of the detector since they are calculated from the measured multiplicity distribution of particles. To recover the true SFM from the experimentally measured one, the efficiency correction is calculated via the cell-by-cell method [43], which assumes a binomial response of the TPC and TOF detectors [43, 45–47]. According to the detector simulations in the STAR experiment, the detector response is close enough to the binomial distributions within statistical significance up to the 6th-order cumulants [3, 13, 48]. The cell-by-cell method is verified by encoding the tracking efficiency of the detector into a cascade ultrarelativistic quantum molecular

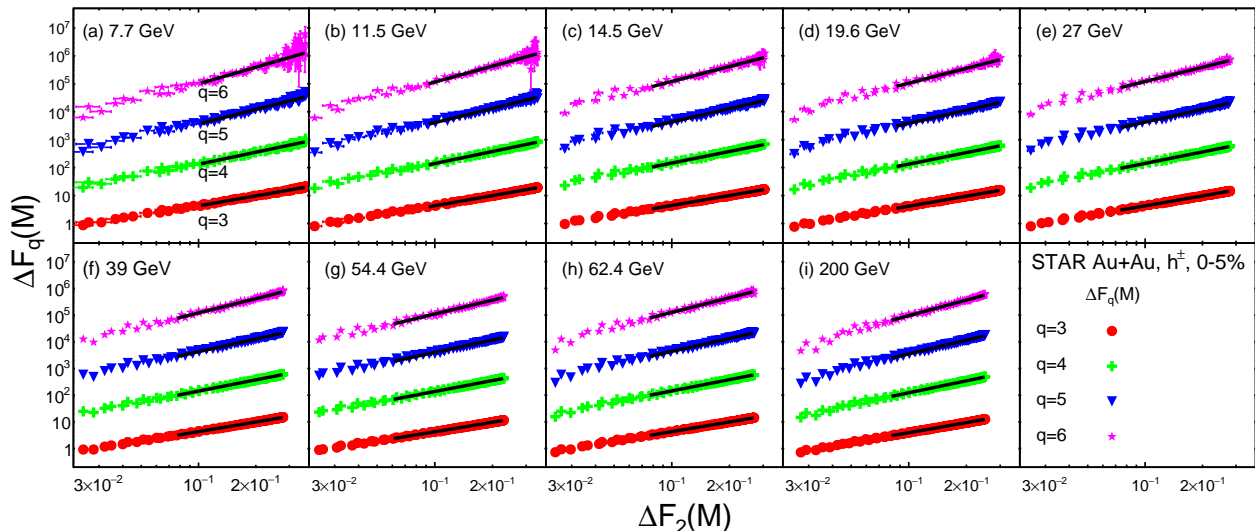


FIG. 2. (a)-(i) $\Delta F_q(M)$ ($q = 3-6$) as a function of $\Delta F_2(M)$ in the most central Au+Au collisions at $\sqrt{s_{NN}} = 7.7-200$ GeV. The solid black lines represent the best power-law fit of $\Delta F_q(M) \propto \Delta F_2(M)^{\beta_q}$ with a fitting range of $\Delta F_2(M)$ from $M \in [30, 100]$. The value of β_q is the slope of the fitting line.

dynamics (UrQMD) event sample [43]. Statistical uncertainty is estimated using the Bootstrap method [49]. In addition, systematic uncertainties are estimated by varying the fit range of M^2 and the track selection criteria for identified charged hadrons.

We measure the SFMs of identified charged hadrons (h^\pm) combining p , \bar{p} , K^\pm , and π^\pm together. Particle identification is required in order to apply the efficiency correction on the SFMs. The domain $[-p_{x,max}, p_{x,max}] \otimes [-p_{y,max}, p_{y,max}]$ of the transverse momentum plane with $p_{x,max} = p_{y,max} = 2.0$ GeV/c is partitioned into M^2 cells to calculate the SFMs according to Eq. (1). Figure 1 (a)-(d) shows $F_q(M)^{data}$ and $F_q(M)^{mix}$ corrected for reconstruction efficiency, from the second-order to the sixth-order, in the most central (0-5%) Au+Au collisions at $\sqrt{s_{NN}} = 7.7-200$ GeV. The event statistics of BES-I data allow us to calculate $F_q(M)$ up to the sixth order ($q = 6$) and in the range of M^2 from 1 to 100^2 . It is observed that $F_q(M)^{data}$ ($q = 2-6$) are significantly larger than $F_q(M)^{mix}$ in the large M^2 region ($M^2 > 100$) at all $\sqrt{s_{NN}}$. Therefore, $\Delta F_q(M)$ ($F_q(M)^{data} - F_q(M)^{mix}$) is significantly larger than zero in the large M^2 region. $F_q(M)^{data}$ was observed to overlap with $F_q(M)^{mix}$ and $\Delta F_q(M) \approx 0$ from the UrQMD calculations [50], which cannot describe the data presented here, since it does not incorporate any density fluctuations.

In Fig. 1 (e)-(h), the $\Delta F_q(M)$ ($q = 2-6$) are shown as a function of M^2 in the most central (0-5%) collisions at four example energies in the $\sqrt{s_{NN}} = 7.7-200$ GeV range. We find that $\Delta F_q(M)$ ($q = 2-6$) increase with increasing M^2 and become saturated when M^2 is large ($M^2 > 4000$). Therefore, $\Delta F_q(M)$ ($q = 2-6$) does not obey a power-law behavior of $\Delta F_q(M) \propto (M^2)^{\phi_q}$

over the whole range of M^2 . Equivalently, $\Delta F_q(M)/M$ scaling is not valid for the whole range of M^2 . The ϕ_q cannot be extracted in a reliable manner (independently of M^2 range) due to the absence of $\Delta F_q(M)/M$ scaling, therefore we focus on the power-law behavior of $\Delta F_q(M) \propto \Delta F_2(M)^{\beta_q}$ and the scaling exponent.

Figure 2 shows $\Delta F_q(M)$ as a function of $\Delta F_2(M)$ in the most central (0-5%) collisions at $\sqrt{s_{NN}} = 7.7-200$ GeV. We find that $\Delta F_q(M)$ ($q = 3-6$) obey a strict power-law behavior with $\Delta F_2(M)$ in the most central Au+Au collisions. The $\Delta F_q(M)/\Delta F_2(M)$ scaling is observed at all collision energies, since density fluctuations could develop in the first-order phase transition and cross-over transition as well [51]. It is worthwhile to note that one should perform the intermittency analysis only when using SFMs at larger M^2 regions, since the power-law scaling is associated with small momentum scales [22, 25]. The value of β_q is obtained through the best fit as the slope of the straight black line in Fig. 2. We note that β_q did not significantly change when the fitting range was varied.

Figure 3 (a) shows β_q as a function of $q - 1$ in the most central Au+Au collisions at $\sqrt{s_{NN}} = 7.7-200$ GeV. In agreement with theoretical expectation, β_q also obeys a power-law behavior with $q - 1$. The scaling exponent, ν , can be obtained through a power-law fit of $\beta_q \propto (q - 1)^\nu$. Figure 3 (b) shows the extracted ν as a function of $\langle N_{part} \rangle$ in various centralities in Au+Au collisions at $\sqrt{s_{NN}} = 19.6-200$ GeV. We observe that ν decreases monotonically from mid-central (30-40%) to the most central (0-5%) Au+Au collisions. On the other hand, the scaling exponent cannot be extracted in various mid-central collisions (5-10%, 10-20%, ...) at $\sqrt{s_{NN}} =$

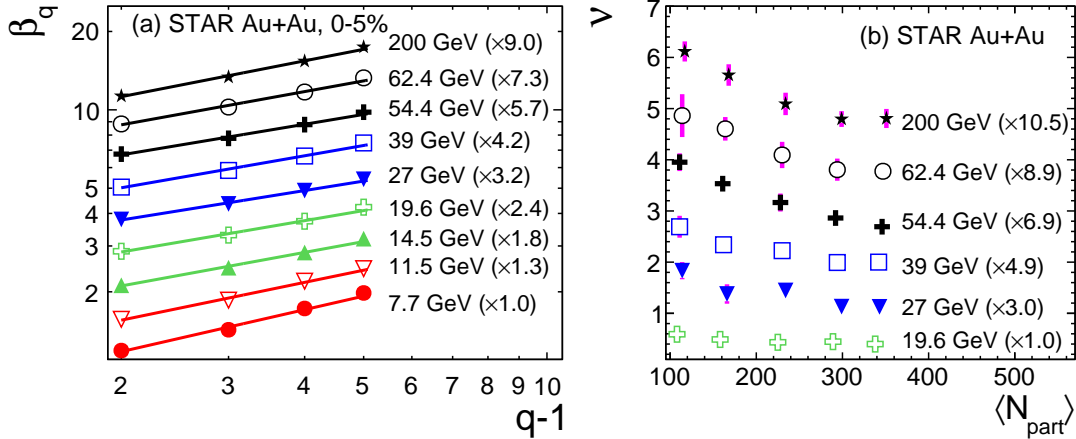


FIG. 3. (a) The scaling index, β_q ($q = 3-6$), as a function of $q - 1$ in the most central (0-5%) Au+Au collisions at $\sqrt{s_{NN}} = 7.7-200$ GeV. The solid lines represent the best power-law fit of $\beta_q \propto (q - 1)^\nu$. The statistical uncertainties of β_q are smaller than the marker size. (b) The scaling exponent (ν), as a function of average number of participant nucleons ($\langle N_{part} \rangle$), in Au+Au collisions at $\sqrt{s_{NN}} = 19.6-200$ GeV. The data with the largest number of $\langle N_{part} \rangle$ correspond to the most central collisions (0-5%), and the rest of the points are for 5-10%, 10-20%, 20-30% and 30-40% centrality, respectively. The systematic uncertainties of ν are shown in bars and the statistical uncertainties are smaller than the marker size. Both β_q and ν at all energies are scaled by different factors.

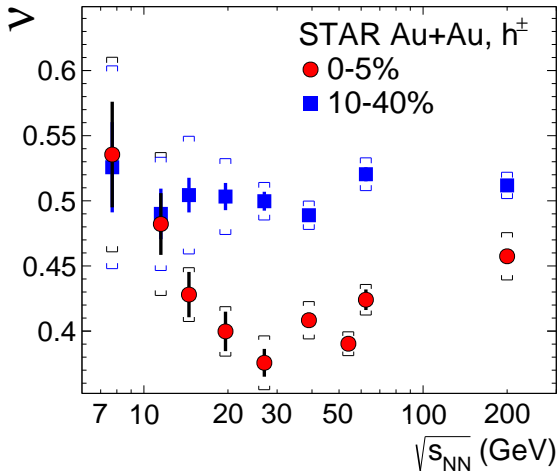


FIG. 4. Energy dependence of the scaling exponent, ν , for identified charged hadrons (h^\pm) in Au+Au collisions at $\sqrt{s_{NN}} = 7.7-200$ GeV. Red circles and blue squares represent ν in the most central collisions (0-5%) and central collisions (10-40%), respectively. The statistical and systematic errors are shown in bars and brackets, respectively.

7.7-14.5 GeV and peripheral collision (40-80%) at $\sqrt{s_{NN}} = 7.7-200$ GeV, since the higher orders of $\Delta F_q(M)$ ($q = 5-6$) exhibit very large statistical uncertainties. The rest of the results will be presented with a merged centrality bin (10-40%) as a baseline to be compared with the most central (0-5%) collisions.

Figure 4 shows the energy dependence of ν for identified charged hadrons in Au+Au collisions for two collision centralities (0-5% and 10-40%). In the most central collisions, ν exhibits a non-monotonic behavior as a function of collision energy and reaches a possible minimum around $\sqrt{s_{NN}} = 27$ GeV. On the other hand, ν is consistent with a constant with increasing $\sqrt{s_{NN}}$ in 10-40% central collisions. At $\sqrt{s_{NN}} \leq 11.5$ GeV, systematic and statistical uncertainties for ν are large. Higher statistics data from the BES-II program [9] will help confirm the energy dependence of ν . The observed value of ν is much smaller than the theoretical prediction of the critical $\nu = 1.30$ from GL theory and 1.0 from the 2D Ising model. One must note that these calculations naturally use the entire phase space without any constraint on acceptance, while the measurements utilize only the experimentally available region of transverse momentum space within η and p_T acceptance. Theoretical calculations with a reduced transverse momentum phase space and equivalent experimental acceptance would be necessary to understand the measured scaling exponent. The transport-based UrQMD model fails to calculate ν due to the absence of $\Delta F_q(M)/\Delta F_2(M)$ scaling [50] and a new model possessing $\Delta F_q(M)/\Delta F_2(M)$ scaling is needed to produce a model baseline.

In summary, we have presented the first measurement of intermittency in heavy-ion collisions at RHIC. The transverse momentum phase space (p_x, p_y) scaled factorial moments of identified charged hadrons combining p, \bar{p}, K^\pm , and π^\pm within $|\eta| < 0.5$ have been calculated up to the sixth order in Au+Au collisions at $\sqrt{s_{NN}} = 7.7-$

200 GeV. With background subtraction, a distinct scaling behavior between the higher-order and second-order scaled factorial moments, $\Delta F_q(M)/\Delta F_2(M)$ scaling, is observed in Au+Au collisions at all energies. Based on the scaling behavior, the extracted scaling exponent, ν , decreases monotonically from the peripheral to the central Au+Au collisions. The ν is consistent with a constant for different collision energies in the mid-central (10-40%) collisions. A non-monotonic energy dependence is observed in the 0-5% most central collisions with ν reaches a possible minimum around $\sqrt{s_{NN}} = 27$ GeV. Whether the observed non-monotonic behavior is related to the CEP or not, detailed calculations from dynamical modelling of heavy-ion collisions with a realistic equation of state are needed.

We thank the RHIC Operations Group and RCF at BNL, the NERSC Center at LBNL, and the Open Science Grid consortium for providing resources and support. This work was supported in part by the Office of Nuclear Physics within the U.S. DOE Office of Science, the U.S. National Science Foundation, National Natural Science Foundation of China, Chinese Academy of Science, the Ministry of Science and Technology of China and the Chinese Ministry of Education, the Higher Education Sprout Project by Ministry of Education at NCKU, the National Research Foundation of Korea, Czech Science Foundation and Ministry of Education, Youth and Sports of the Czech Republic, Hungarian National Research, Development and Innovation Office, New National Excellency Programme of the Hungarian Ministry of Human Capacities, Department of Atomic Energy and Department of Science and Technology of the Government of India, the National Science Centre of Poland, the Ministry of Science, Education and Sports of the Republic of Croatia, German Bundesministerium für Bildung, Wissenschaft, Forschung und Technologie (BMBF), Helmholtz Association, Ministry of Education, Culture, Sports, Science, and Technology (MEXT) and Japan Society for the Promotion of Science (JSPS).

[1] A. Bzdak, S. Esumi, V. Koch, J. Liao, M. Stephanov, and N. Xu, *Phys. Rept.* **853**, 1 (2020), 1906.00936 [nucl-th].

[2] X. Luo, Q. Wang, N. Xu, and P. Zhuang, eds., *Properties of QCD Matter at High Baryon Density* (Springer, 2022).

[3] J. Adam *et al.* (STAR), *Phys. Rev. Lett.* **126**, 092301 (2021), arXiv:2001.02852 [nucl-ex].

[4] X. Luo and N. Xu, *Nucl. Sci. Tech.* **28**, 112 (2017), arXiv:1701.02105 [nucl-ex].

[5] Y. Aoki, G. Endrődi, Z. Fodor, S. D. Katz, and K. K. Szabo, *Nature* **443**, 675 (2006), arXiv:hep-lat/0611014.

[6] S. Ejiri, *Phys. Rev. D* **78**, 074507 (2008), arXiv:0804.3227 [hep-lat].

[7] E. S. Bowman and J. I. Kapusta, *Phys. Rev. C* **79**, 015202 (2009), arXiv:0810.0042 [nucl-th].

[8] Y. Hatta and M. A. Stephanov, *Phys. Rev. Lett.* **91**, 102003 (2003).

[9] STAR Note 0598: BES-II whitepaper. <https://drupal.star.bnl.gov/STAR/starnotes/public/sn0598>.

[10] M. Mačkowiak-Pawłowska (NA61/SHINE), *Nucl. Phys. A* **1005**, 121753 (2021), arXiv:2002.04847 [nucl-ex].

[11] T. Ablyazimov *et al.* (CBM), *Eur. Phys. J. A* **53**, 60 (2017), arXiv:1607.01487 [nucl-ex].

[12] L. Adamczyk *et al.* (STAR), *Phys. Rev. Lett.* **112**, 032302 (2014), arXiv:1309.5681 [nucl-ex].

[13] M. Abdallah *et al.* (STAR), *Phys. Rev. C* **104**, 024902 (2021), arXiv:2101.12413 [nucl-ex].

[14] L. Adamczyk *et al.* (STAR), *Phys. Rev. Lett.* **112**, 162301 (2014), arXiv:1401.3043 [nucl-ex].

[15] L. Adamczyk *et al.* (STAR), *Phys. Rev. C* **92**, 014904 (2015), arXiv:1403.4972 [nucl-ex].

[16] R. A. Lacey, *Phys. Rev. Lett.* **114**, 142301 (2015), arXiv:1411.7931 [nucl-ex].

[17] A. S. K. N. G. Antoniou, F. K. Diakonov and K. S. Kousouris, *Phys. Rev. Lett.* **97**, 032002 (2006).

[18] R. C. Hwa and M. T. Nazirov, *Phys. Rev. Lett.* **69**, 741 (1992).

[19] E. A. De Wolf, I. M. Dremin, and W. Kittel, *Phys. Rept.* **270**, 1 (1996).

[20] A. Bialas and R. C. Hwa, *Phys. Lett. B* **253**, 436 (1991).

[21] H. Satz, *Nucl. Phys. B* **326**, 613 (1989).

[22] N. G. Antoniou, F. K. Diakonov, X. N. Maintas, and C. E. Tsagkarakis, *Phys. Rev. D* **97**, 034015 (2018), arXiv:1705.09124 [hep-ph].

[23] N. G. Antoniou, Y. F. Contoyiannis, F. K. Diakonov, A. I. Karanikas, and C. N. Ktorides, *Nucl. Phys. A* **693**, 799 (2001), arXiv:hep-ph/0012164.

[24] N. G. Antoniou, N. Davis, and F. K. Diakonov, *Phys. Rev. C* **93**, 014908 (2016), arXiv:1510.03120 [hep-ph].

[25] T. Anticic *et al.* (NA49), *Phys. Rev. C* **81**, 064907 (2010), arXiv:0912.4198 [nucl-ex].

[26] J. Wu, Y. Lin, and Y. W. Li, Zhiming, *Phys. Lett. B* **801**, 135186 (2020), arXiv:1901.11193 [nucl-th].

[27] T. Anticic *et al.* (NA49), *Eur. Phys. J. C* **75**, 587 (2015), arXiv:1208.5292 [nucl-ex].

[28] N. G. Antoniou, Y. F. Contoyiannis, F. K. Diakonov, and G. Mavromanolakis, *Nucl. Phys. A* **761**, 149 (2005), arXiv:hep-ph/0505185.

[29] A. Bialas and R. B. Peschanski, *Nucl. Phys. B* **273**, 703 (1986).

[30] A. Bialas and R. B. Peschanski, *Nucl. Phys. B* **308**, 857 (1988).

[31] D. Prokhorova and N. Davis (NA61/SHINE), *Universe* **5**, 103 (2019).

[32] R. C. Hwa, *Phys. Rev. D* **47**, 2773 (1993).

[33] R. C. Hwa and C. B. Yang, *Phys. Rev. C* **85**, 044914 (2012), arXiv:1111.6651 [nucl-th].

[34] W. Ochs and J. Wosiek, *Phys. Lett. B* **214**, 617 (1988).

[35] W. Ochs, *Z. Phys. C* **50**, 339 (1991).

[36] A. Kamal, N. Ahmad, and M. M. Khan, *Acta Phys. Polon. B* **46**, 1549 (2015).

[37] Z. Cao, Y. Gao, and R. C. Hwa, *Z. Phys. C* **72**, 661 (1996), arXiv:nucl-th/9601011.

[38] L. Adamczyk *et al.* (STAR), *Phys. Rev. C* **96**, 044904 (2017), arXiv:1701.07065 [nucl-ex].

[39] K. H. Ackermann *et al.* (STAR), *Nucl. Instrum. Meth. A* **499**, 624 (2003).

[40] W. J. Llope (STAR), *Nucl. Instrum. Meth. A* **661**, S110 (2012).

- [41] L. Adamczyk *et al.* (STAR), *Phys. Rev. Lett.* **113**, 092301 (2014), [arXiv:1402.1558 \[nucl-ex\]](#).
- [42] M. L. Miller, K. Reygers, S. J. Sanders, and P. Steinberg, *Ann. Rev. Nucl. Part. Sci.* **57**, 205 (2007), [arXiv:nucl-ex/0701025](#).
- [43] J. Wu, Y. Lin, Z. Li, X. Luo, and Y. Wu, *Phys. Rev. C* **104**, 034902 (2021), [arXiv:2104.11524 \[nucl-th\]](#).
- [44] Z. Li, *Mod. Phys. Lett. A* **37**, 2230009 (2022), [arXiv:2203.01490 \[nucl-th\]](#).
- [45] X. Luo, *Phys. Rev. C* **91**, 034907 (2015), [Erratum: *Phys.Rev.C* 94, 059901 (2016)], [arXiv:1410.3914 \[physics.data-an\]](#).
- [46] X. Luo and T. Nonaka, *Phys. Rev. C* **99**, 044917 (2019), [arXiv:1812.10303 \[physics.data-an\]](#).
- [47] T. Nonaka, M. Kitazawa, and S. Esumi, *Phys. Rev. C* **95**, 064912 (2017), [Erratum: *Phys.Rev.C* 103, 029901 (2021)], [arXiv:1702.07106 \[physics.data-an\]](#).
- [48] M. Abdallah *et al.* (STAR), *Phys. Rev. Lett.* **127**, 262301 (2021), [arXiv:2105.14698 \[nucl-ex\]](#).
- [49] B. Efron and R. Tibshirani, *Statist. Sci.* **1**, 54 (1986).
- [50] J. Wu, Z. Li, X. Luo, M. Xu, and Y. Wu, *Phys. Rev. C* **106**, 054905 (2022), [arXiv:2209.07135 \[nucl-th\]](#).
- [51] N. G. Antoniou and F. K. Diakonou, *J. Phys. G* **46**, 035101 (2019), [arXiv:1802.05857 \[hep-ph\]](#).